X-611-68-450
PREPRINT



# OBSERVATIONS OF COSMIC RAY ELECTRONS BETWEEN 2.7 AND 21.5 MEV

G. M. SIMNETT
F. B. McDONALD



NOVEMBER 1968

GSFC
GODDARD SPACE FLIGHT CENTER
GREENBELT, MARYLAND

# Observations of Cosmic Ray Electrons Between 2.7 and 21.5 MeV

by

G. M. Simnett*

and

F. B. McDonald

November 1968

NASA/Goddard Space Flight Center
Greenbelt, Maryland

*NAS/NASA Postdoctoral Resident Research Associate

# Observations of Cosmic Ray Electrons Between 2.7 and 21.5 MeV

by

G. M. Simnett* and F. B. McDonald

NASA/Goddard Space Flight Center
Greenbelt, Maryland

## Abstract

Results are presented from the IMP-IV satellite on the 2.7 - 21.5 MeV electron intensity in interplanetary space between July 3rd and August 27th 1967. The measured electron intensity is believed to be uncontaminated by solar electrons. The analysis procedure for background subtraction and subsequent derivation of the electron spectrum is described. The results of electron accelerator calibrations are used extensively. The origin of the electrons is discussed, and the results are compared with the predicted intensity of knock-on electrons from proton-electron collisions in interstellar space. The measured electron spectrum is shown to be compatible with a sole origin in the galactic knock-on component if solar modulation of low energy electrons is insignificant. The electron energy spectrum obtained is well represented by a power law of the form $dJ/dE = 132\ E^{-1.75}$ electrons/$m^2$ sec sr MeV between 2.7 and 21.5 MeV.

*NAS/NASA Postdoctoral Resident Research Associate

## Introduction

A direct observation of the low energy electron component of cosmic rays in interplanetary space has been made with a dE/dx vs. E scintillator telescope on-board the IMP-IV satellite (Explorer 34). The differential energy spectrum of the electrons has been measured in the energy interval 2.7 - 21.5 MeV. The results reported here cover the time period July 3rd - August 27th, 1967, which was chosen because of the low level of solar activity. The particles from the solar electron event between 08.00 and 15.00 UT on July 5, 1967 have been excluded from the analysis. The apogee of IMP-IV was at around 216,000 km during the period under discussion. Data are excluded when the satellite was below 70,000 km and over 80% of the data are taken from outside 125,000 km. The axis of the detector is normal to the ecliptic plane.

The first measurement of electrons in this energy interval was made by Cline, Ludwig and McDonald (1964) with a detector on-board the IMP-I satellite. Our results were obtained from a similar detector, but a more sophisticated analysis technique was employed than for the IMP-I data, which not only makes a more precise background subtraction but extends the energy range covered by the detector.

It is intended that the electron flux studied here is representative of the equilibrium galactic flux, perhaps modulated by solar activity, but without contamination from either solar or terrestrial electrons. At the present time it is not certain whether or not there is a quiescent solar electron intensity at relativistic energies.

A study of the long term time variation of the electron intensity will be very informative in establishing the magnitude of such a solar component. However, the short term variations reported by Cline and McDonald (1968) display an inverse correlation with solar activity and $K_p$ and a strong positive correlation with the high energy galactic nucleons as observed by the Deep River Neutron Monitor. Forbush decreases have also been observed in the low energy component. This supports the view that this component is of galactic origin. The earth is also a copious source of low energy electrons in the form of albedo. This source has been discounted because of the lack of any spatial variation in intensity over the IMP-IV orbit. However, it must be remembered that this does not automatically exclude the earth as the origin of low energy interplanetary electrons. It is the purpose of this paper to present the data and to discuss briefly the source mechanism under the assumption that the electrons are of galactic origin. An examination of cosmic ray electron and positron measurements from 3 MeV to 10 GeV (see Ramaty and Lingenfelter, 1968, for a summary of data above 100 MeV ) suggest there must be at least three sources of cosmic ray electrons.

Above .5 GeV, the $e^+/e^-$ ratio is on the order of or less than 0.1. Most of the electrons are of primary origin and must be directly accelerated in appropriate source regions. The measured positron flux (Hartman, 1967) is in reasonable agreement with that expected from the decay of charged pions produced by cosmic ray nucleon-nucleon collision in the galaxy. Below 0.5 GeV the $e^+/e^-$ ratio increases, which

suggests that electrons from charged pion decay become more important in this energy region. A third source which is important in the 3 - 20 MeV region is the Coulomb interaction between cosmic ray nucleons and electrons in the interstellar medium. At ~15 MeV the electron intensity from $\pi \rightarrow \mu \rightarrow e$ and Coulomb collisions should be equal. Below 15 MeV the knock-on contribution should dominate. The role played by primary electrons in the low energy region is not clear. However the intensity and energy spectra of the low energy component are consistent with a knock-on source if solar modulation effects are small.

Other possible sources such as beta decay of radioactive nuclei and neutron decay will contribute, mainly at energies below a few MeV. The Fermi process may be capable of accelerating thermal electrons up to relativistic energies, and interstellar $\gamma$ rays can produce Compton electrons. Abraham, Brunstein and Cline (1966) were able to calculate the contributions of several of these processes, and concluded that the most probable sources were knock-on electrons or thermal electrons accelerated by the Fermi process. The revised flux values presented here suggest that it is not necessary to invoke the Fermi process if the effects of solar modulation are small.

The Detector

The detector used for these measurements is of the same design as that flown on the earlier satellites IMP-I, II and III, and it has been described in detail elsewhere (Bryant, Ludwig and McDonald, 1962). The cross section of the detector is shown in Figure 1. The front element is a thin CsI (Tl) crystal which serves as a dE/dx detector, and this is operated in coincidence with a thick CsI (Tl) crystal which serves as an E - dE/dx detector. An anticoincidence guard counter of plastic scintillator surrounds the E - dE/dx detector. For convenience this element will hereafter be referred to as the E detector. A matrix of dE/dx versus E is generated for particles which satisfy the dE/dx · E coincidence requirement and do not trigger the guard counter. Electrons produce a pulse in dE/dx equal to or very close to that of a singly charged minimum ionizing particle; there is no confusion between electrons and protons or helium nuclei which are detected normally. However, there is a considerable background of counts in the "electron" part of the matrix which must be subtracted before the true electrons can be identified. The origin of the background is now discussed.

Any minimum ionizing proton which produces a dE/dx · E coincidence but does not trigger the guard counter may be mistaken for an electron. There are two ways in which this can happen; the guard counter may have an efficiency $< 1$ or the proton may interact in the E scintillator in such a way that no charged particle penetrates into the guard counter. An inefficiency in the guard counter would produce a peak in the matrix corresponding to minimum or near minimum ionization loss in both dE/dx and E.

This follows from the fact that the majority of singly charged cosmic rays which can penetrate the detector are minimum ionizing. Such a peak cannot be resolved in the data, and we have neglected guard counter inefficiency as a source of background.

The other main source of background comes from $\gamma$ radiation, either primary or locally produced in the spacecraft. It is relevant that the dE/dx scintillator has a thickness of 0.05 radiation lengths and the E scintillator a thickness of 1.03 radiation lengths. The primary $\gamma$ ray intensity above 1 MeV has an upper limit $\approx 3 \times 10^{-2}$ cm$^{-2}$ sr$^{-1}$ sec$^{-1}$ (see Anand, Daniel and Stephens, 1968, for review of data) and it obeys a power law spectrum with index $\approx -2$. The background produced by such an intensity is negligible. Therefore we need only consider $\gamma$ rays produced in the spacecraft as a source of $\gamma$ ray background.

A $\gamma$ ray can produce a coincidence count in the detector in the following ways:

(1) The $\gamma$ ray can undergo a Compton interaction in both the dE/dx and E scintillators. For low energy $\gamma$ rays the photoelectric effect is important, but for the purpose of this discussion it may be included under Compton interactions. These events are peaked in a region of the matrix corresponding to small energy loss in both dE/dx and E.

(2) The $\gamma$ ray can undergo a Compton interaction in one scintillator such that the Compton electron is sufficiently energetic to satisfy the coincidence requirement.

(3) The $\gamma$ ray can undergo pair production such that either one or both of the electron pair produces a coincidence count. If pair production takes place in E, both electrons may emerge through dE/dx and the event will be placed in a region of the matrix corresponding to 2x minimum ionizing.

Clearly combinations of Compton interactions and pair production can also produce background counts.

The energy spectrum of Compton electrons is softer than the energy spectrum of the parent $\gamma$ rays. The Compton electrons are produced predominantly in the E detector and can only be detected if they subsequently pass through dE/dx. As the Compton electron spectrum is expected to be soft, the majority of electrons will have energies less than $\approx$ 3 MeV when they enter dE/dx. Accelerator calibration has shown that up to energies of 3 MeV the most probable energy loss in dE/dx is close to the total kinetic energy of the electron. Thus, counts from Compton electrons are characterized in the matrix by a small energy loss in E and a diffuse energy loss in dE/dx. Incident primary electrons have a more sharply defined energy loss in dE/dx, as they must emerge with sufficient energy to trigger the E detector.

The important points to realize with respect to the background events discussed above are as follows:

(1) Background from proton interactions and from pair production is concentrated along the minimum ionizing, or electron line of the matrix, with perhaps a slight enhancement at 2x minimum ionizing due to electron pairs.

(2) Background from Compton electrons is concentrated in low E channels and is not sharply peaked at the minimum ionizing line in dE/dx.

Interactions in dE/dx which send one or more charged particles into E and yet do not trigger the guard counter produce a more general type of background where the outputs of dE/dx and E are variable and unrelated.

This defines the origin of the background events which need to be eliminated from the raw data. The following section describes the detector response to electrons and shows in detail how the background subtraction is made.

The Background Subtraction

A detector identical to that flown on IMP-IV has been extensively calibrated using 2.3 - 4.0 MeV electrons from the Van de Graaff accelerator at the National Bureau of Standards, Gaithersburg, and 3 - 40 MeV electrons from the linear accelerator at the Naval Research Laboratory, Washington, D. C. The efficiency of the detector for analyzing electrons is shown in Figure 2 as a function of energy. A separate pulse height analysis was performed on the output of dE/dx at energies below 4 MeV to investigate the number of electrons which stop in the dE/dx scintillator.

Above 4 MeV efficiency is defined as the ratio of the number of coincidence counts unaccompanied by a guard counter pulse to the total number of coincidence counts, on the assumption that all electrons incident within the acceptance cone of the detector produce a dE/dx · E coincidence. This neglects scattering in dE/dx with the argument that the number of electrons incident within the acceptance cone which are scattered outside the geometry is balanced by electrons incident outside the acceptance cone which are scattered into the geometry.

Figure 2 shows that the detector efficiency reaches a peak at 5 MeV and slowly falls up to 20 MeV. The reasons for this are apparent if one considers the type of interaction an electron might undergo in passing through CsI, which has a radiation length of 1.89 cm. (The thickness of the E scintillator is 1.93 cm, or 1.03 radiation lengths.)

(1) The electron may be scattered into the guard counter from the E scintillator.

(2) A photon formed by the bremsstrahlung process may produce and electron-positron pair or a Compton electron near the edge of the E scintillator: such electrons can trigger the guard. The photon may interact in the guard counter itself. The linear absorption coefficient for 2 MeV $\gamma$ rays is 0.2 $cm^{-1}$ in CsI.

(3) Above 12 MeV an electron which does not radiate may reach the guard counter from range considerations.

All the above processes lead to a gradual fall in detector efficiency with increasing electron energy.

Above 20 MeV the most probable bremsstrahlung loss is such that the residual range of the electron is large enough to penetrate the guard counter (Berger & Seltzer, 1964). This leads to a change in slope of the efficiency versus incident energy curve at 20 MeV. The efficiency does not fall to zero as an electron may still radiate an energetic photon which leaves the E detector without interacting.

The effect of the random nature of the bremsstrahlung process on the amount of energy deposited in the E scintillator is of interest. There is a probability for any energy deposition from zero to the full electron kinetic energy on entry to the E scintillator. Zero energy deposition occurs if the electron radiates all its energy into a single photon which escapes from the detector system without interacting. The full electron energy is deposited if the electron initiates an electron-photon cascade which is completely absorbed in the E scintillator.

These facts are confirmed by the calibration data. Figure 3a shows the calibration matrix obtained for a beam of 6 $\pm$ 0.1 MeV electrons and Figure 3b shows typical single parameter pulse height distributions for 3, 6, 16, and 30 MeV electrons as a function of channel number in E.

The ordinate in Figure 3b is arbitrary in the interests of clarity. The channel width is 0.65 MeV/channel in terms of energy deposited in the crystal. The energy indicated on each histogram in Figure 3b is the electron energy on entry to dE/dx. It should be noted that the most probable energy loss in E is a decreasing percentage of the incident energy as the latter is increased.

The electron calibration illustrates that the counts in a single channel cannot be allocated a specific energy, as electrons can produce counts in all channels up to or very close to that corresponding to their maximum energy. Also the percentage of counts in a given channel which correspond to electrons of known energy cannot be established immediately as this depends on the energy distribution, or spectrum, of the electrons responsible for the counts. Therefore we adopted an iterative procedure for the analysis which generated a calibration matrix for a postulated incident electron spectrum and compared this matrix with the data. This is described in detail below.

Figure 2 and Figure 3b show that the probability of having electron counts beyond $\approx$ channel 50 in E is very low, even for a flat electron spectrum. Channel 50 would correspond to an energy deposition greater than 32.5 MeV in a crystal which has a thickness of 1.89 g $cm^{-2}$. Therefore all counts in the matrix beyond channel 50 in E which produce a near minimum ionizing pulse in dE/dx must be background. Figure 4 shows the raw data profiles in dE/dx channel space for different E channels. The profiles for channels 51-60, 61-70, 71-80 are similar, whereas the profiles for channels below 30 show a sharper peak corresponding to the inclusion of genuine electron counts. The electron counts were

obtained by subtracting from the raw data the background count profile established from data in E channels 51-80. The normalization condition imposed was that the resultant profile, that we attribute to electrons, must have the same shape in dE/dx channel space as the calibration data. In the lowest three channels in E the shape of the background profile was modified to take into account the increasing importance of Compton electrons. In all cases the absolute requirement was that the resultant counts attributed to incident electrons should have the same distribution in dE/dx channel space as the calibration data.

The profile in dE/dx channel space from the calibration data is insensitive to the shape of the spectrum used to generate the calibration matrix. The differential energy spectrum is defined as

$$\frac{dJ(E)}{dE} = k(E)\ E^{-\gamma(E)}$$

where E is the electron kinetic energy, J(E) is the intensity, k(E) is a normalizing factor and $\gamma(E)$ is the index of the spectrum. Figure 5 shows profiles in dE/dx channel space for two sample spectra, $\gamma = 2.0$ and $\gamma = 0.5$. Also shown in Figure 5 is the resultant data profile after subtraction of the background. This profile is sensitive to the shape and normalization of the background profile. The error in the number of counts under the resultant profile is determined by the maximum deviation of the background profile which can be tolerated before the shape of the resultant profile is in disagreement with the calibration data. The error changes from typically 20% in channel 3, 15% in

channel 7 to 25% in channels 20 - 24. We estimate these figures to be equivalent to 2 standard deviations.

The satellite data show that background counts caused by $\gamma$ rays interacting in both scintillators A and B are concentrated in low E channels. Thus the contribution by such events to the overall background in high E channels, which provide the background profile, is very small. Therefore a preliminary correction for this type of event was applied to the data using a profile from a calibration made with a $\gamma$ ray beam up to 3.8 MeV. This profile was normalized to the peak in channel 2 (dE)/dx and subtracted from the raw data; the result for channel 3 (E) is shown in Figure 6.

Thus far the analysis has subtracted the background to leave a matrix distribution of the form demanded by the calibration, i.e., with a given distribution of counts as a function of dE/dx channel number. Any succeeding analysis may therefore be confined to a single parameter, namely the distribution of counts as a function of E channel number.

One further subtraction must be made before the electron spectrum can be calculated, which is the contribution in low E channels from electrons above the maximum calibration energy. Figure 3b shows that electrons have a finite response in all channels up to a maximum which depends on their initial energy; this cannot be ignored. There are three important characteristics of such a correction:

(1) It is sensitive to the interplanetary electron spectrum.

(2) It is peaked around E channel number 20. It was emphasized above that the main reason high energy electrons are counted is because they lose a large fraction of their

energy to a $\gamma$ ray, or rays, and thus become equivalent in the detector to lower energy electrons. Irrespective of the shape of the interplanetary electron spectrum this correction is negligible for channels below channel 12, and cannot influence the results below around 12 MeV.

(3) There is negative feedback to the correction from the final computed electron spectrum. If the postulated electron intensity >40 MeV used to calculate the correction is too large, the correction itself will be too large, which will depress the corrected data in the 20 MeV region such that an extrapolation to beyond 40 MeV is incompatible with the postulated intensity. The opposite is true if the postulated intensity >40 MeV is too small.

The magnitude of the correction which was finally applied to the data was $\approx$ 20% in channel 20 (E).

The calibration data were now used to find a spectrum which produced a fit to the corrected satellite data. This was achieved by the following iterative procedure. A matrix was generated by summing the calibration matrices for different energies according to the following equation:

$$\text{Final matrix} = \sum_E \left(\frac{dJ}{dE}\right)_E \quad (\text{Efficiency (E)}) \quad (\Delta E)$$

$$(GF(Eo)/GF(E)) \quad (\text{Calibration matrix (E)})$$

dJ/dE is the proposed spectrum, $\Delta E$ is the width of the energy interval and $GF(E_o)/GF(E)$ is the ratio of the detector geometry factors for the threshold energy $E_o$ and E. The geometry factor as a function of energy was computed using the electron range as a function of energy derived from the data of Berger and Seltzer (1964). The values of E are

pre-determined by the energies at which the calibration was performed. Limits were placed on the proposed spectrum which restricted it a form such that $d^2J/dE^2$ was both continuous and negative. This precludes any fine structure to the spectrum. If the final matrix did not agree with the corrected satellite data within the errors the postulated spectrum was changed, with appropriate changes to the corrected satellite data, until a fit was obtained. The contribution by each E channel to a given energy interval was evaluated, and the final electron intensity as a function of energy was obtained. This is plotted in Figure 7a.

We have endeavored to explain precisely how the final result was obtained. There is one point which should be mentioned in connection with the computed spectrum. No distinction is made between electrons and positrons. The term "electron" is used to describe both negatrons and positrons unless the latter are specifically named, in which case "electron" refers to the negative component.

Discussion

Recent reports of the low energy electron intensity are summarized in Figure 7b. The results of Webber (1968a), Beedle and Webber (1968) were obtained from high altitude balloon flights. Those of Cline, Ludwig and McDonald (1964) were from the IMP-I satellite, and those of Fan, Gloeckler, Simpson and Verma (1968) were from the IMP-III satellite. There is general agreement below 20 MeV. It must be stressed that the apparent change in intensity between the IMP-I and IMP-IV results must not be interpreted as a real time variation. The analysis procedure for the two sets of data was not the same, although the detectors were basically identical. The IMP-I results are being re-analyzed and the time variation of the electron intensity will be reported in a later paper.

The spectrum shown in Figure 7a may be compared with the intensity of knock-on electrons from proton - electron collisions in the interstellar medium predicted by Abraham, Brunstein and Cline (1966). They calculate an equilibrium knock-on electron spectrum in the galaxy $dJ/dE = 0.066\ ds/dE\ E^{-1.76}$ $(cm^2\ sec\ sr\ MeV)^{-1}$ where dE/dx is the ionization loss in the interstellar medium. The ionization losses in neutral hydrogen and helium are 4.25 MeV $g^{-1}$ $cm^2$ and 2.01 MeV $g^{-1}$ $cm^2$ respectively for 7 MeV electrons (Berger and Seltzer, 1964). These values are slightly energy dependent, increasing towards higher energies. The presence of helium in the interstellar gas is offset to a first approximation by the fact that the medium is 5 - 10% ionized (Ginzburg and Syrovatsky, 1964). A value of $dE/dx = 4.25$ MeV $g^{-1}$ $cm^2$ is uncertain

by $\approx$ 20%. The interstellar knock-on electron spectrum calculated by Abraham et al. does not have to make any assumptions about solar modulation of low energy cosmic rays. Knock-on electrons between 3 MeV and 20 MeV are produced predominantly by protons with energies above $\approx$ 2 GeV and solar modulation of these particles is negligible for the purpose of this discussion. The calculation is also independent of the density of interstellar matter.

The knock-on electron spectrum without correction for solar modulation is shown in Figure 7a as the dashed lines. It is immediately apparent that this is very close to the observed spectrum. The implications of this depend on the degree of solar modulation of low energy electrons and also on their charge ratio.

Recent measurements by Cline and Hones (1968) give an upper limit to the positron intensity between 0.5 MeV and 3 MeV which is in itself consistent with an extrapolation of the IMP-IV spectrum to low energies. It is difficult to postulate a source mechanism for the production of such a high positron intensity at 1 MeV. $\pi^{+} - \mu^{+} - e^{+}$ decay and pair production may be neglected. One hypothesis is the decay of radioactive isotopes such as $N^{12}$ (16.3 MeV), $O^{14}$ (4.1, 1.8 MeV) etc. However, the cross sections for production of energetic positron emitters are low, and this process is unlikely to yield an important intensity of positrons above 3 MeV. In view of the production difficulty and the fact that the Cline and Hones measurement is an upper limit, the contribution of low energy positrons to the present results is neglected.

We have shown that the unmodulated proton-electron knock-on intensity is sufficient to supply the measured electron intensity. It is worthwhile to consider the contribution from other sources in this energy region. Figure 8 shows the calculated equilibrium electron intensity from $\pi - \mu - e$ decay, e($\pi$), (Ramaty and Lingenfelter, 1968); the electron-electron knock-on intensity, (e - e), (Ramaty, 1968); the proton-electron knock-on intensity (p - e), (Abraham et al, 1966); and the neutron decay electron intensity, e(n), (Ramaty and Lingenfelter, 1966). The (p - e) knock-on intensity includes the contribution from cosmic rays of $Z \geq 2$ and it is calculated for a value of $dE/ds = 4.25$ MeV $g^{-1}$ $cm^2$. The $\pi - \mu - e$ decay spectrum is calculated for a value of $X_o = 4$ g $cm^{-2}$, where $X_o$ is the mean amount of matter traversed by cosmic rays. The neutron decay spectrum is in agreement with the estimate made by Abraham et al (1966). It is interesting to note that if knock-on production and $\pi - \mu - e$ decay are the dominant mechanisms at low energies, an $e^+/e^-$ ratio of . 5 would be predicted at ~15 MeV. Confirmation of this would be important for the model outlined here. The electron-electron knock-on intensity was calculated from the measured electron spectrum at earth, demodulated assuming a modulation function of the form

$$f = \begin{cases} e^{-\eta/R_o\beta}, & \eta = 0.4, \quad R_o = 0.5 \text{ GV}, \quad R < R_o \\ e^{-\eta/R\beta} & R > R_o \end{cases}$$

where R is the electron rigidity in GV. This is the only secondary component that is sensitive to the modulation function. However, unless

the electron modulation is far greater than predicted, this is not a major electron source. On this model the modulation of electrons at low rigidities depends on the ratio $\eta/R_o$. The recent review paper by Webber (1968b) suggests that $R_o$ is $\approx$ 1 GV, based on a study of time variations of protons and helium nuclei. Gloeckler and Jokipii (1967) propose an upper limit to the modulation parameter $\eta$ of 1 GV from interstellar energy density requirements. This places an upper limit on $\eta/R_o \approx 1$, which is close to the value used by Ramaty.

A comparison of the predicted (unmodulated) total secondary electron intensity, $e_s$, with the data shows a divergence with increasing energy which is mainly attributed to the dominance of $\pi - \mu - e$ decay electrons above 20 MeV. The calculations of $e(\pi)$ are estimated to be accurate to within around 50% (Ramaty, 1968) if it is assumed that $X_o = 4$ g cm$^{-2}$ is a reasonable value. Charge ratio measurements of Hartman (1967) suggest that this source is not dominant above 200 MeV which would favor a reduction in $e(\pi)$. The dotted line in Figure 8 indicates the magnitude of the total secondary component if $e(\pi)$ is reduced by a factor of 2. We interpret this as a reasonable lower limit to the total equilibrium electron intensity in interstellar space.

It is evident from Figure 8 that modulation of electrons at 15 MeV is larger than modulation at 3 MeV. At 3 MeV the predicted value of $\eta/R_o$ is $0.2 \pm 0.2$, while at 15 MeV we obtain $\eta/R_o = 0.9 \pm 0.2$. This assumes all of the low energy electrons are of secondary origin.

In summary, we have measured an electron intensity which is well represented by a power law of the form

$$\frac{dJ}{dE} = 132\ E^{-1.75}\ \text{electrons/m}^2\ \text{sec sr MeV}$$

between 2.7 MeV and 21.5 MeV. This is in good agreement with the predicted knock-on electron intensity in this energy range.

## References


Abraham, P. B., K. A. Brunstein and T. L. Cline, 1966, Phys. Rev., 150, 1088.

Anand, K. C., R. R. Daniel and S. A. Stephens, 1968, Can. J. Phys., 46, S484.

Beedle, R. E. and W. R. Webber, 1968, Can. J. Phys., 46, S1014.

Berger, M. J. and S. M. Seltzer, 1964, NASA Document SP-3012.

Bryant, D. A., G. H. Ludwig, and F. B. McDonald, 1962, I.R.E. Transactions on Nuclear Science NS-9, 376.

Cline, T. L. and E. W. Hones, 1968, Can. J. Phys., 46, S527.

Cline, T. L., G. H. Ludwig and F. B. McDonald, 1964, Phys. Rev. Ltr., 13, 786.

Fan, C. Y., G. Gloeckler, J. A. Simpson and S. D. Verma, 1968, Ap. J., 151, 737.

Ginzburg, V. L. and S. I. Syrovatsky, 1964, The Origin of Cosmic Rays, Macmillan, New York, p. 118.

Gloeckler, G. and J. R. Jokipii, 1967, Ap. J. Ltr., 148, L 41.

Hartman, R. C., 1967, Ap. J., 150, 371.

Ramaty, R. and R. E. Lingenfelter, 1966, J. Geophys. Res., 71, 3687.

Ramaty, R. and R. E. Lingenfelter, 1968, Phys. Rev. Ltr., 20, 120.

Ramaty, R., 1968, private communication.

Webber, W. R., 1968a, J. Geophys. Res., 73, 4912.

Webber, W. R., 1968b, Proc. 10th Int'l. Conf. on Cosmic Rays, A146.

## Figure Captions

Figure 1: Schematic cross section of the detector.

Figure 2: The detector efficiency as a function of electron energy obtained from electron accelerator calibration.

Figure 3a: The two dimensional pulse height analysis matrix obtained from a beam of 6 $\pm$ 0.1 MeV electrons. The matrix is the sum of three matrices obtained for incident angles of 0°, 10° and 23° of the electron beam to the axis of the detector.

Figure 3b: Single parameter pulse height distributions for 3, 6, 16 and 30 MeV electrons as a function of channel number in E - dE/dx.

Figure 4: Pulse height distributions in dE/dx channel space from the IMP-IV raw data for the time period July 3 - August 27, 1967. Solid lines are fitted to data from channels 51-60, 61-70, and 71-80 in E - dE/dx. The uppermost line shows how the line profile is fitted to data from channels 20-24. In this case the difference between the line and the data points gives an upper limit to the electron contribution from these channels.

Figure 5: Electron accelerator calibration profiles in dE/dx channel space are shown for representative E - dE/dx channels. Profiles are illustrated for two power law spectra with $\gamma$ = 0.5 and 2.0 (see text). Background corrected data from IMP-IV is compared with the calibration data.

Figure 6: The pulse height distribution in dE/dx channel space from the $\gamma$ ray calibration at 3.8 MeV is compared with raw data from IMP-IV. The peak in the $\gamma$ ray profile is normalized to the raw data in channel 2 (dE)/dx. In channel 3 the $\gamma$ ray point and the raw data point are coincident.

Figure 7: (a) The measured differential energy spectrum for electrons from July 3 to August 27, 1967. The straight lines are predicted knock-on electron intensities in interstellar space computed by Abraham et al (1966) for two values of electron ionization loss. The errors shown are a combination of statistical errors and errors from the analysis procedure.

(b) Recent observations of primary electrons between 2.7 MeV and 40 MeV.

Figure 8: The calculated equilibrium secondary electron spectrum in interstellar space is plotted as $e_s$. The p - e component is the knock-on electron spectrum from protons and $Z \geq 2$. Similarly e - e is the knock-on electron spectrum from electrons. e(n) is the neutron decay electron spectrum and e($\pi$) is the $\pi$ - $\mu$ - e decay spectrum. The dotted line is the total secondary electron spectrum if e($\pi$) is reduced by a factor of 2. $X_o$ is the integrated path length for cosmic rays in g $cm^{-2}$ and dE/dx is the ionization loss in interstellar space.

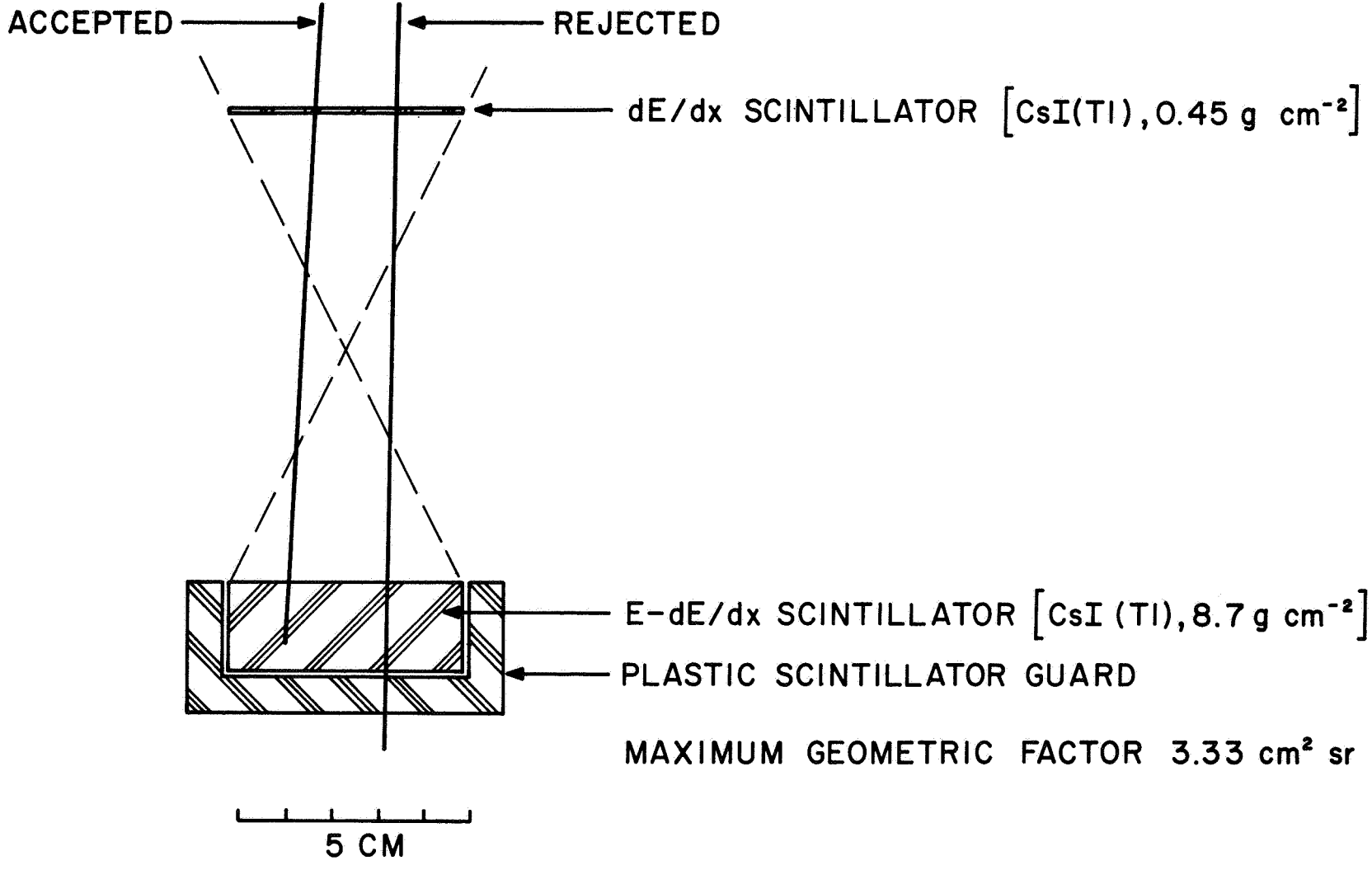
ACCEPTED
REJECTED
dE/dx SCINTILLATOR [CsI(Tl), 0.45 g cm⁻²]
E-dE/dx SCINTILLATOR [CsI (Tl), 8.7 g cm⁻²]
PLASTIC SCINTILLATOR GUARD
MAXIMUM GEOMETRIC FACTOR 3.33 cm² sr
5 CM

Figure 1

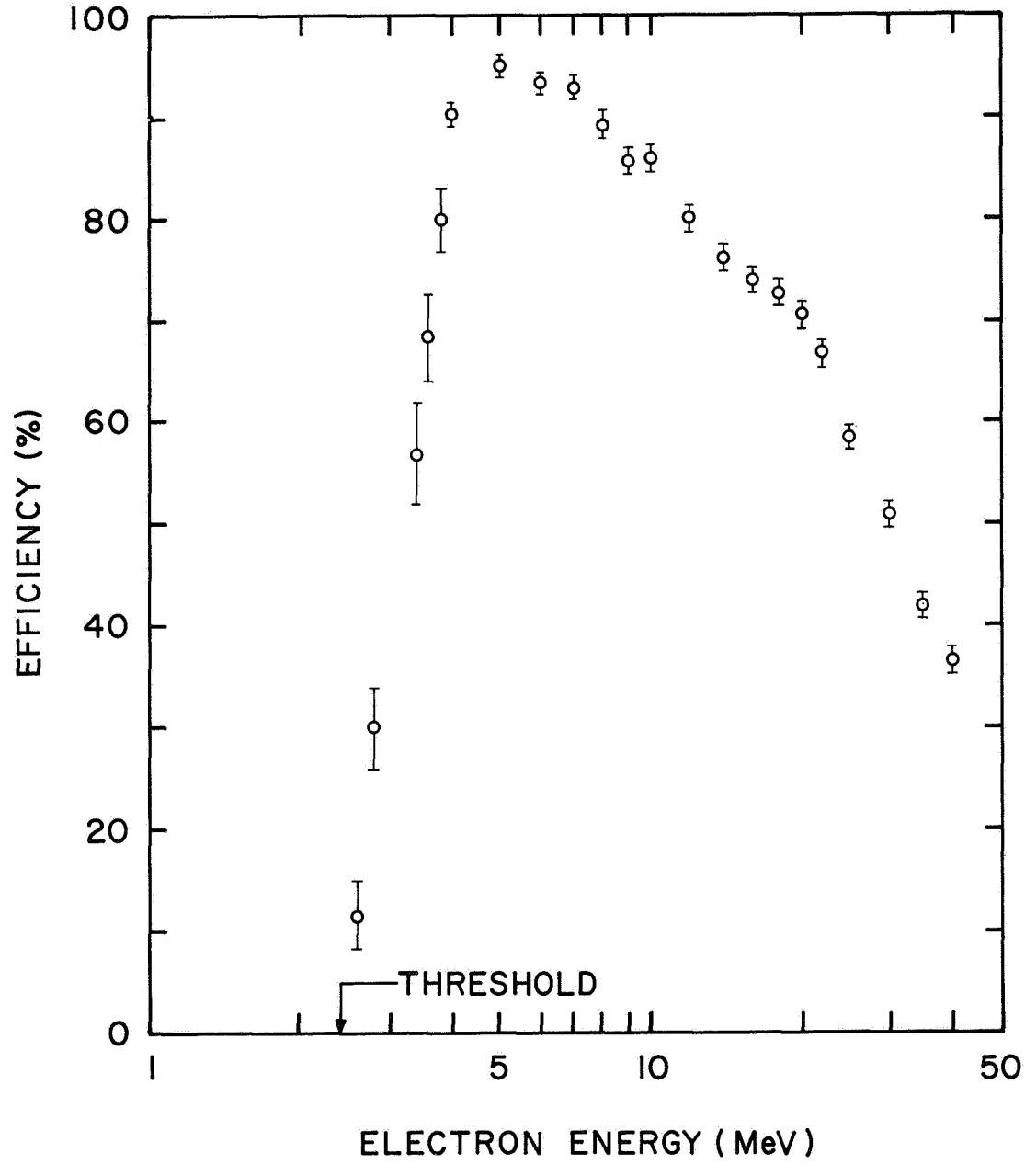
100
80
60
40
20
0
EFFICIENCY (%)
THRESHOLD
1
5
10
50
ELECTRON ENERGY (MeV)

Figure 2

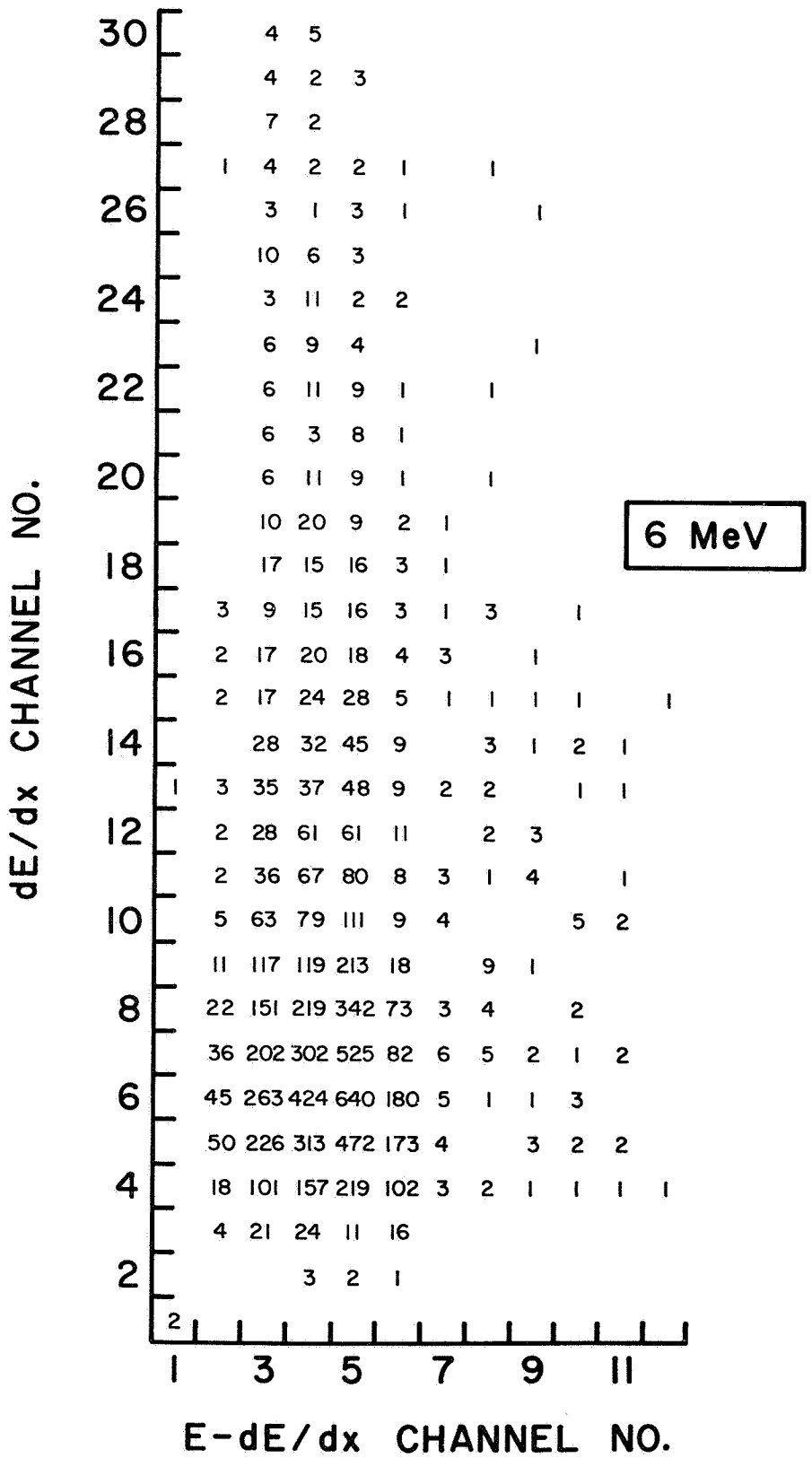
6 MeV
dE/dx CHANNEL NO.
E-dE/dx CHANNEL NO.
30
28
26
24
22
20
18
16
14
12
10
8
6
4
2
1
3
5
7
9
11

Figure 3a

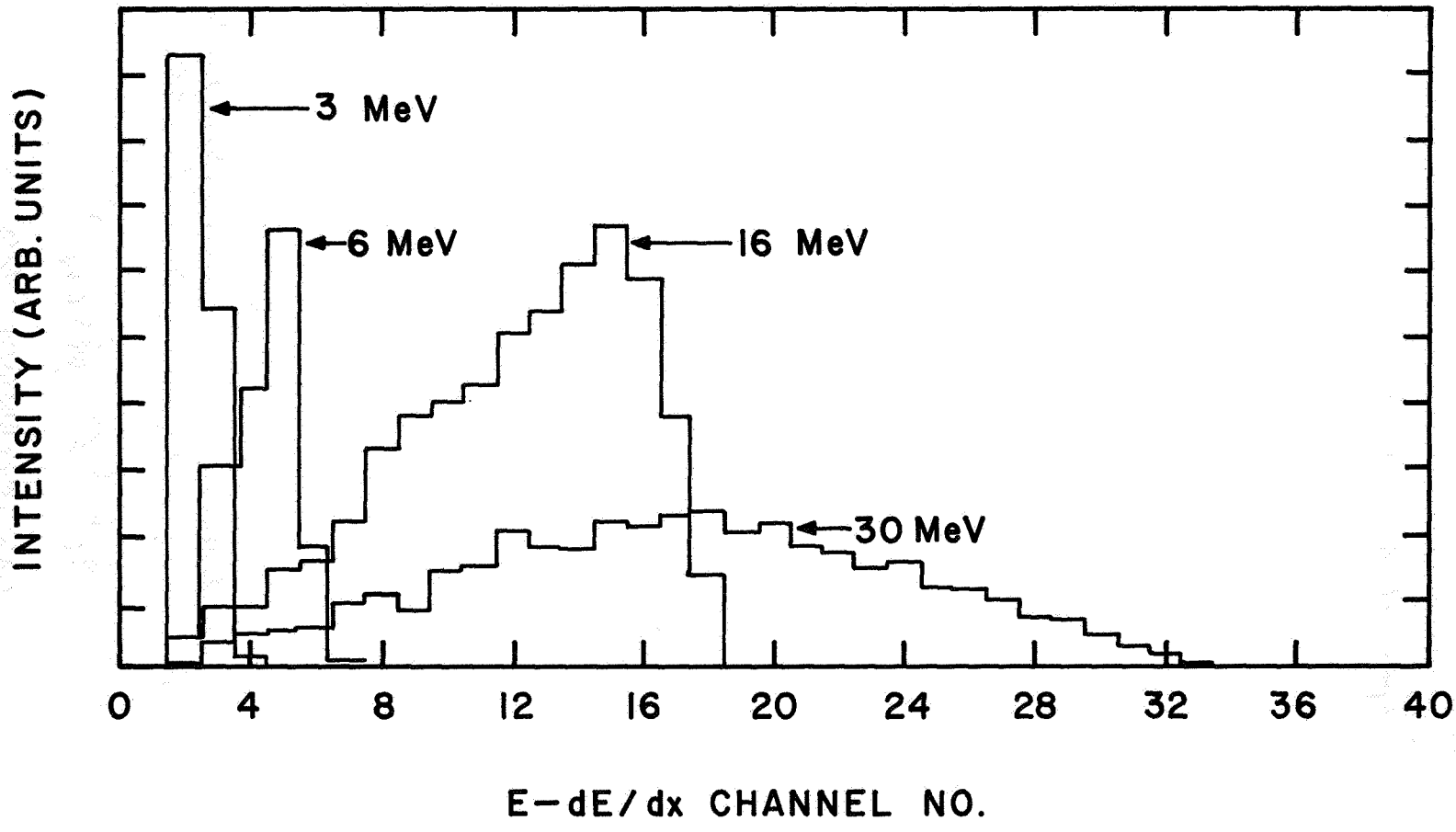
INTENSITY (ARB. UNITS)
3 MeV
6 MeV
16 MeV
30 MeV
0
4
8
12
16
20
24
28
32
36
40
E−dE/dx CHANNEL NO.

Figure 3b

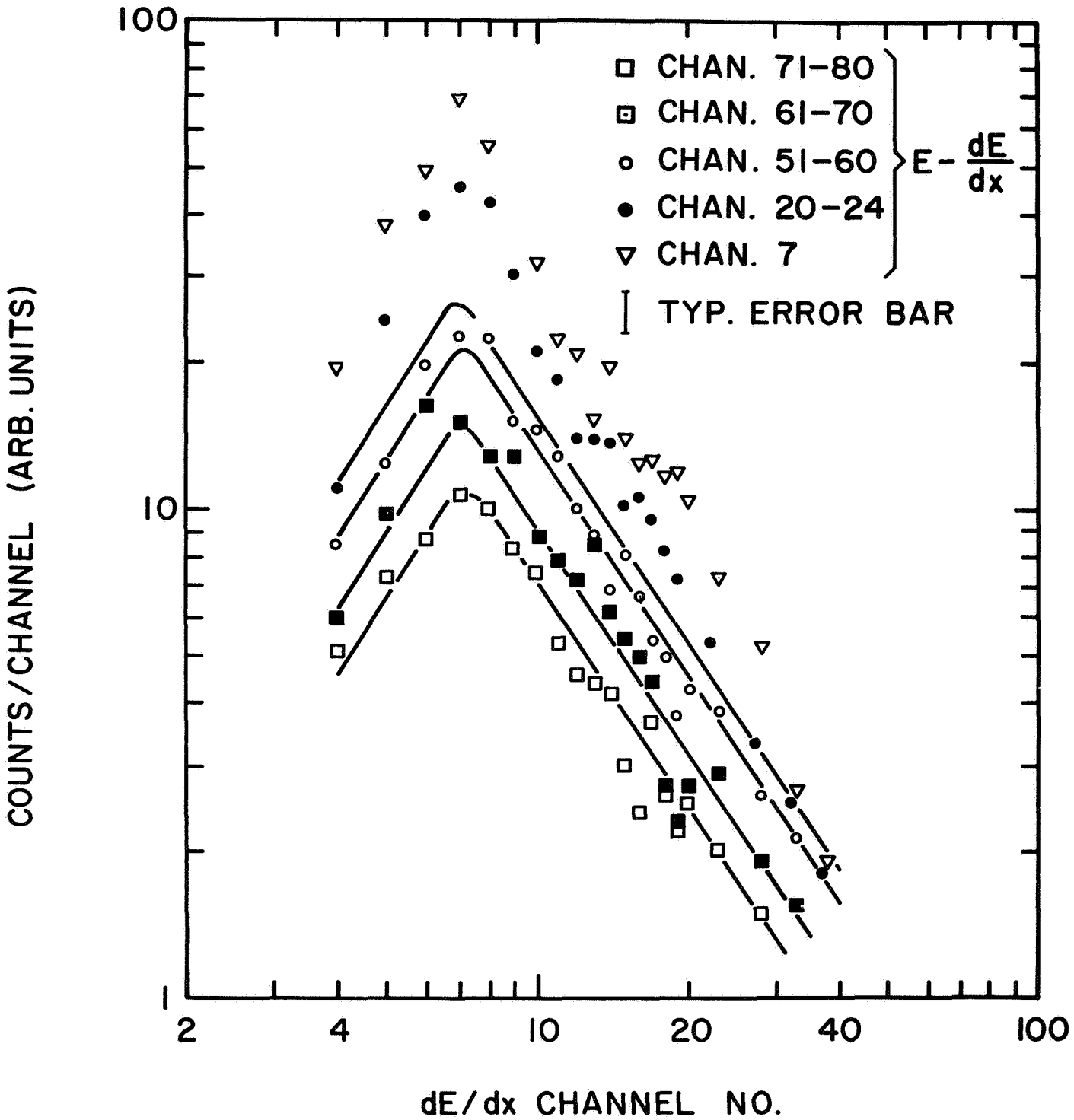
100
10
1
2
4
10
20
40
100
CHAN. 71-80
CHAN. 61-70
CHAN. 51-60
CHAN. 20-24
CHAN. 7
E- dE/dx
TYP. ERROR BAR
COUNTS/CHANNEL (ARB. UNITS)
dE/dx CHANNEL NO.

Figure 4

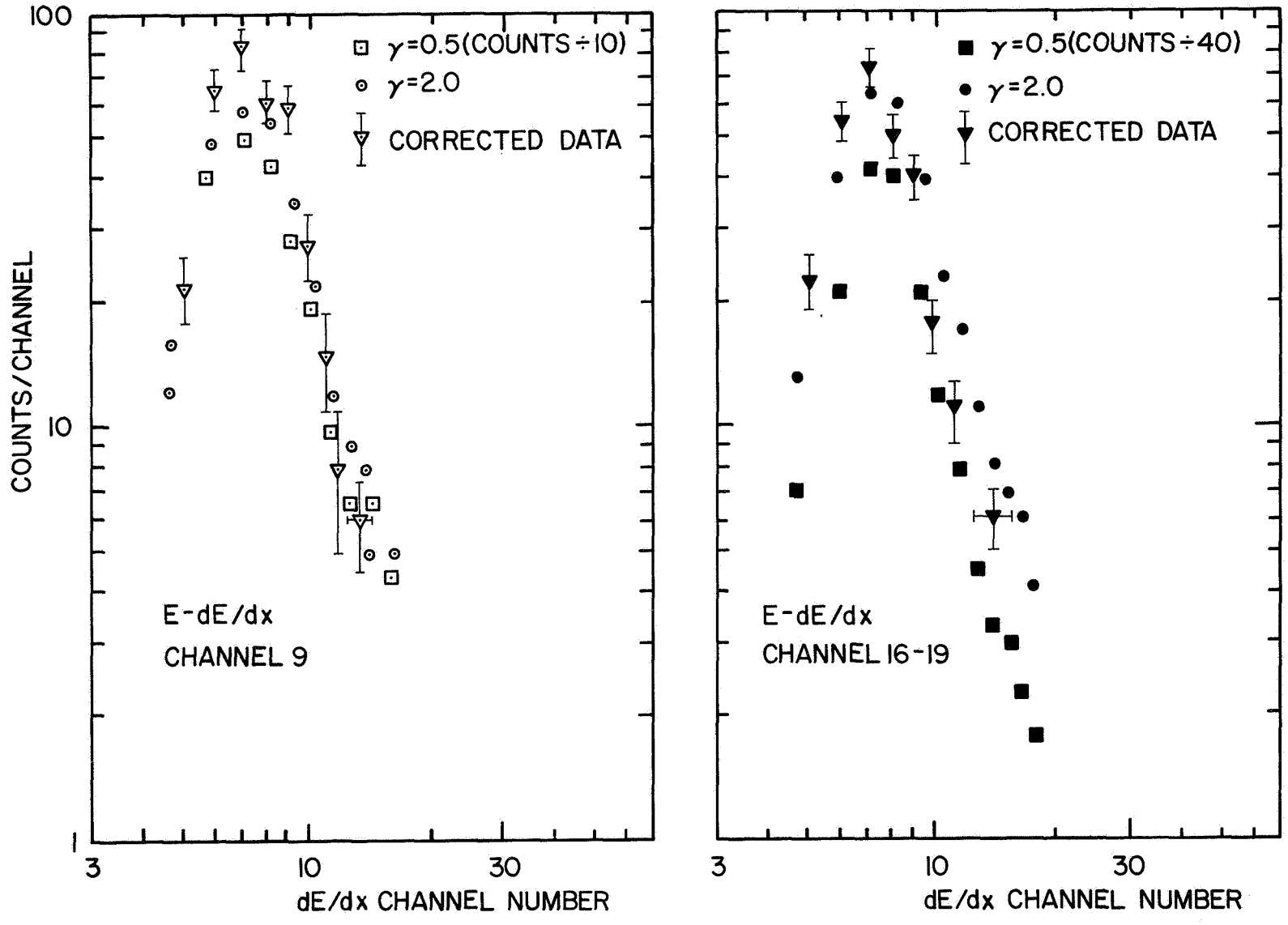
100
10
1
COUNTS/CHANNEL
γ=0.5(COUNTS÷10)
γ=2.0
CORRECTED DATA
E-dE/dx
CHANNEL 9
3
10
30
dE/dx CHANNEL NUMBER
γ=0.5(COUNTS÷40)
γ=2.0
CORRECTED DATA
E-dE/dx
CHANNEL 16-19
3
10
30
dE/dx CHANNEL NUMBER

Figure 5

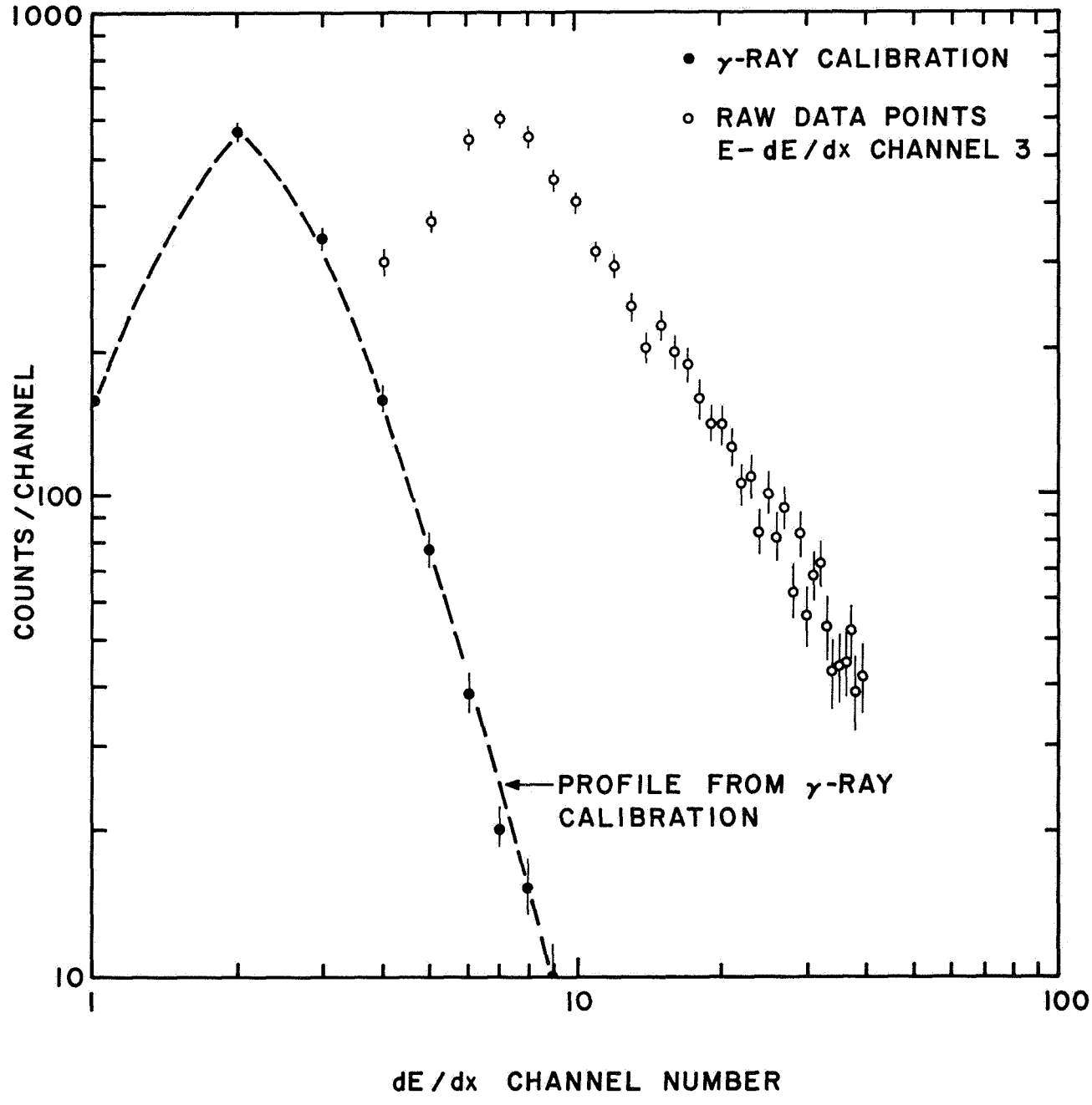
1000
100
10
1
10
100
COUNTS / CHANNEL
dE / dx CHANNEL NUMBER
γ-RAY CALIBRATION
RAW DATA POINTS
E - dE / dx CHANNEL 3
PROFILE FROM γ-RAY
CALIBRATION

Figure 6

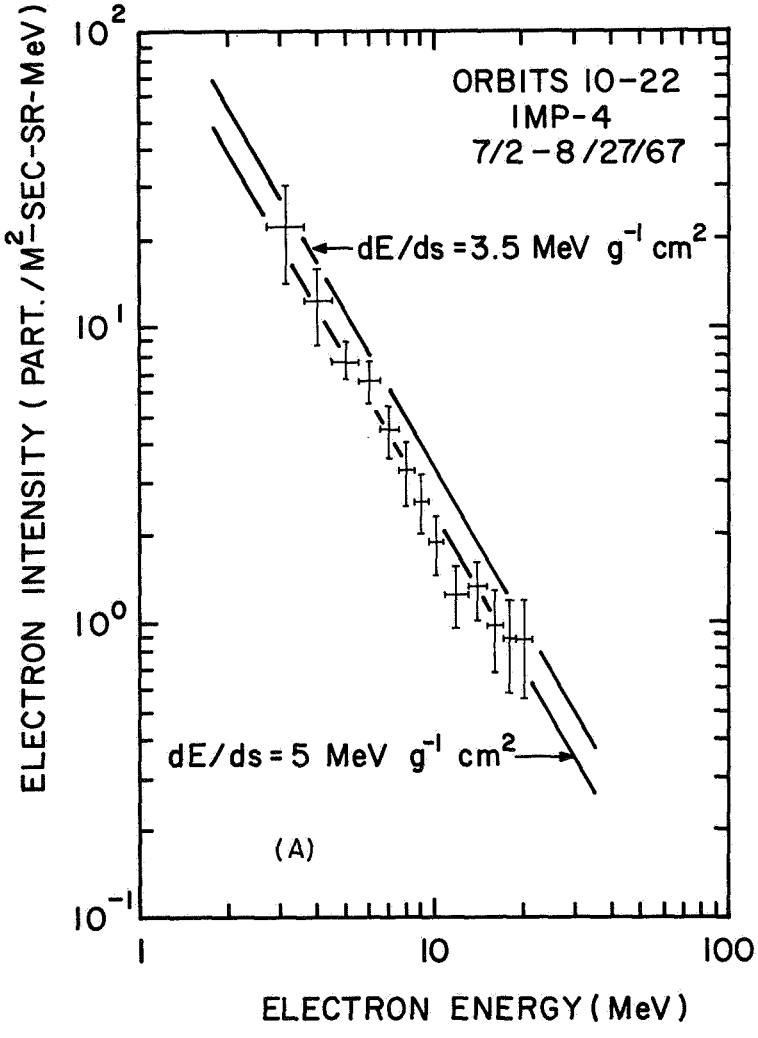


Figure 7a

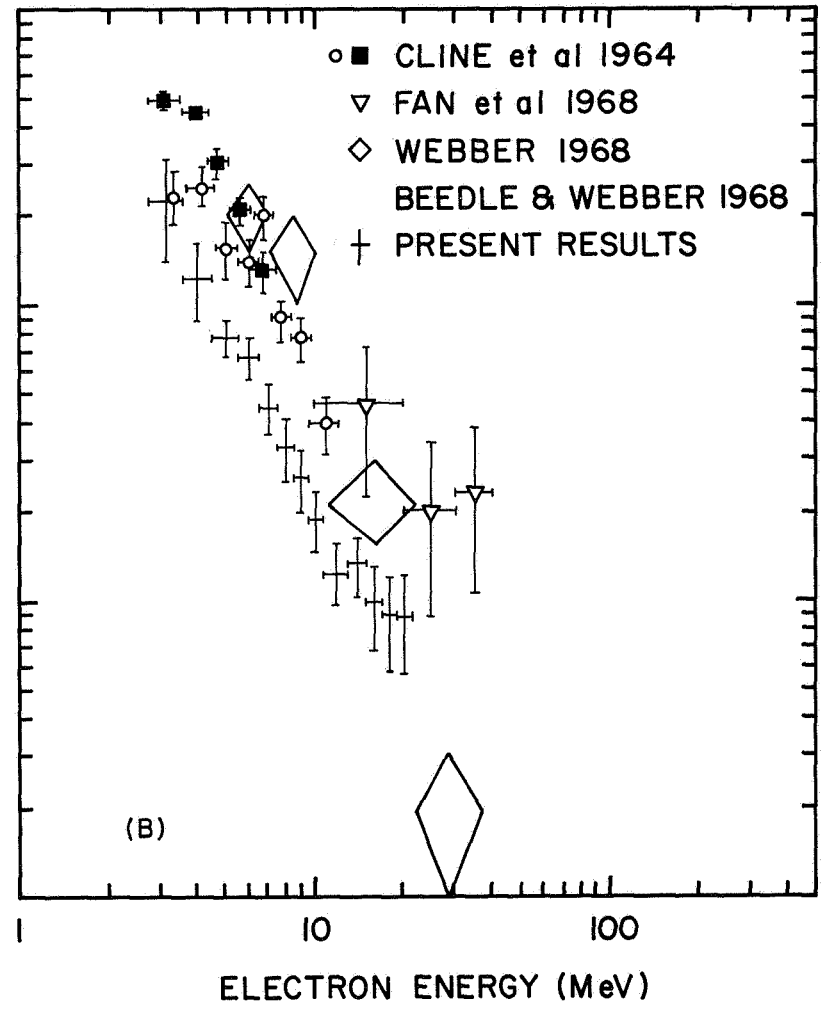


Figure 7b

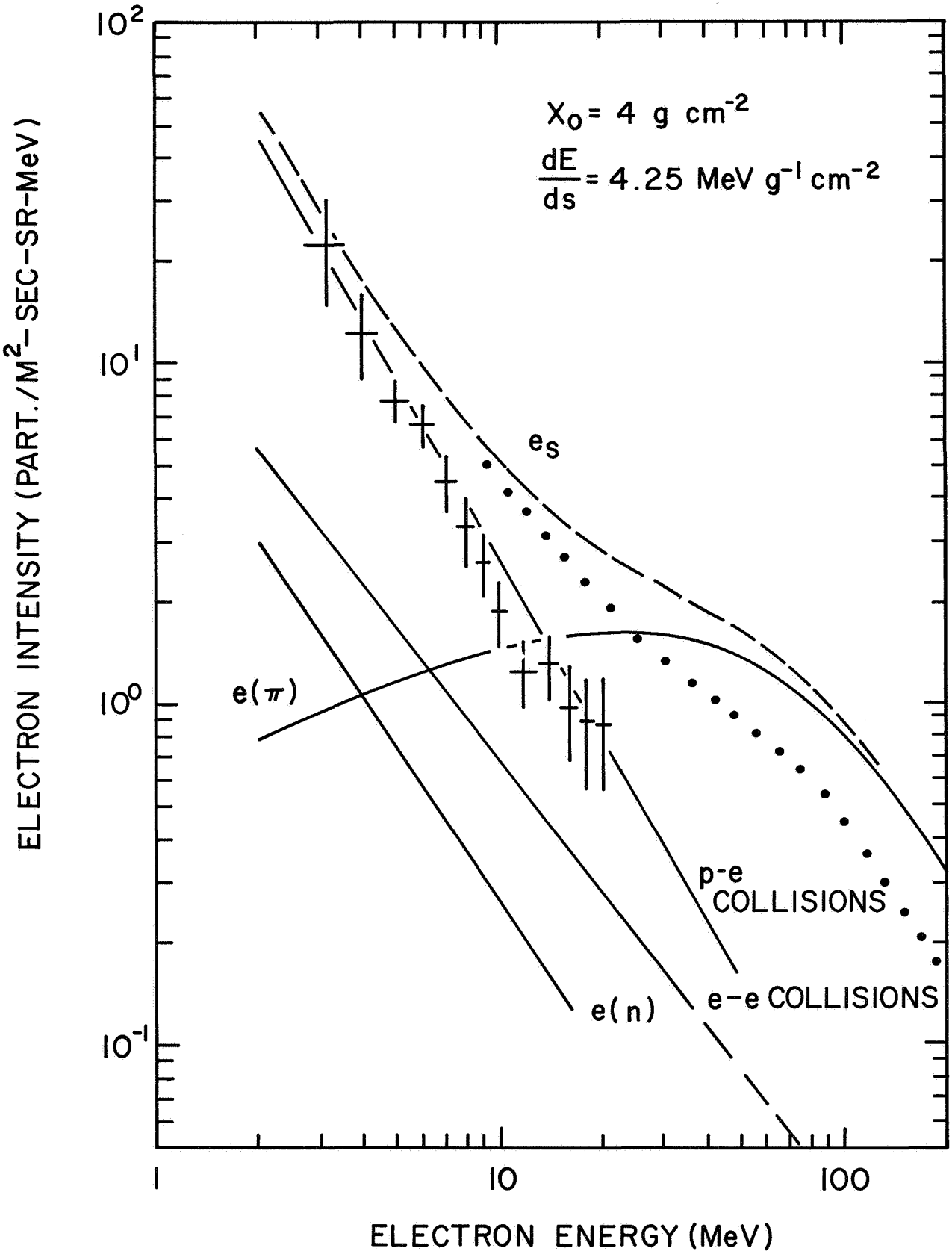
$X_0 = 4$ g cm$^{-2}$
$\frac{dE}{ds} = 4.25$ MeV g$^{-1}$ cm$^{-2}$
$e_s$
$e(\pi)$
e(n)
p-e COLLISIONS
e-e COLLISIONS
$10^2$
$10^1$
$10^0$
$10^{-1}$
1
10
100
ELECTRON INTENSITY (PART./M$^2$-SEC-SR-MeV)
ELECTRON ENERGY (MeV)

FIGURE 8